

Active slosh control and damping - Simulation and experiment

Martin Konopka^{a,*}, Francesco De Rose^a, Hans Strauch^b, Christina Jetzschmann^b, Nicolas Darkow^c, Jens Gerstmann^c



^a ArianeGroup GmbH, Airbus-Allee 1, 28199, Bremen, Germany

^b Airbus Defence & Space GmbH, Airbus-Allee 1, 28199, Bremen, Germany

^c German Aerospace Center (DLR), Institute of Space Systems, Robert-Hooke-Str. 7, 28359, Bremen, Germany

ARTICLE INFO

Keywords:

Sloshing
Computational fluid mechanics
Control
GNC
Coupled simulation

ABSTRACT

Future reignitable cryogenic upper stages perform long ballistic coasting phases in earth orbit. During those coasting phases, the tanks are loaded with liquid propellants and propellant sloshing occurs due to external disturbances or attitude change maneuvers. The sloshing propellant motion induces reaction forces and torques acting on the space vehicle structure, e.g. rocket upper stages. To keep the upper stage at the desired target attitude, the guidance, navigation, and control (GNC) algorithm commands thruster firings to counter the fluid forces. At ArianeGroup (AG), the Final Phase Simulator FiPS aims at simulating the coupling between fluid mechanics, GNC, and rigid body dynamics. To validate the coupling of GNC with linear lateral water sloshing, on ground experiments at the German Aerospace Center's Hexapod sloshing facility were performed. It was demonstrated that the developed control algorithm is able to damp the linear lateral sloshing within 4 s. FiPS simulations of the open and closed loop sloshing experiments showed that the experimental forces are matched with an uncertainty of less than 5% for open loop phases. For closed-loop phases the simulations match the experimental damping intervals with an accuracy of better than 5% and the force amplitude with an accuracy of about 20%.

1. Introduction

The accurate prediction of the attitude evolution of future versatile upper stages is essential to ensure a robust mission design and an accurate delivery of the payloads to the desired target orbits. For such a prediction, it is key to consider the interaction of the propellant sloshing with the rigid body dynamics of the upper stage. To do so, the Final Phase Simulator FiPS¹ was developed at AG. In FiPS, the rigid body dynamics of the upper stage is coupled with the sloshing dynamics in the tanks which is computed by the commercial flow solver Flow-3D v.11.0.4. Furthermore, a control algorithm is fed with the attitude data, i.e. the software is a testbed for GNC development [5], [6]. The FiPS software is currently in use to support the GNC development for the ballistic flight phases of the Ariane 6 upper liquid propulsion module (ULPM) [1], [2]. One of the purposes of FiPS in the framework of upper stage attitude analysis is to identify coupled modes between sloshing and upper stage attitude motion. Such a coupling might occur during the longitudinal spin phase where the propellant and oxidizer accumulates in bulges in the tanks. These results raise the question how to validate FiPS for such phenomena. The current strategy is to perform

two validation steps. First, validate FiPS by on-ground sloshing experiments with control in the loop. Second, validate FiPS by in-orbit sloshing experiments using free-flying tanks aboard the international space station [7]. The first step is presented in the current study. Therefore, the purpose of the current study is twofold. First, on-ground linear lateral sloshing experiments with closed loop control to damp sloshing are performed and the experiments are rebuild with FiPS. Second, the current active damping experiments and simulations are analyzed to show that active sloshing damping by control is feasible for future upper stages. Note that the current on-ground linear lateral sloshing experiments are applicable to orbital phases with low acceleration levels, e.g. settling maneuvers where thrusters fire and where sloshing with a very low frequency occurs. However, to observe the coupled motion of the fluids at longitudinal spin modes such as it is used for upper stages in orbits requires a micro-gravity environment, i.e. the second FiPS validation step using in-orbit experiments [7].

To perform on-ground sloshing experiments with control in the loop the hexapod sloshing system at the Cryo-Lab [13] [14], of the Institute of Space Systems of the German Aerospace Center (DLR) in Bremen, Germany, is used. Using the hexapod system it is possible to simulate a

* Corresponding author.

E-mail addresses: martin.konopka@ariane.group (M. Konopka), hans.strauch@airbus.com (H. Strauch), nicolas.darkow@dlr.de (N. Darkow).

¹ FiPS: registered trademark.

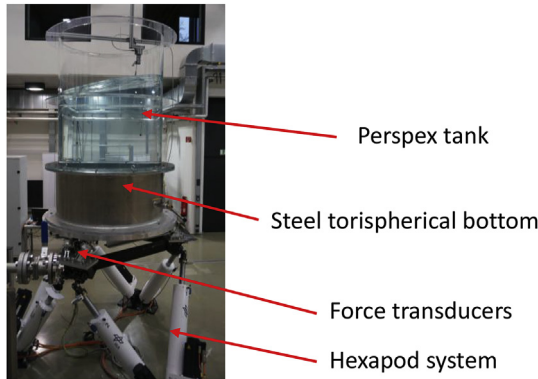


Fig. 1. DLR hexapod with 1.2 m Perspex tank filled with water.

6 degree-of-freedom movement in a normal gravity environment, i.e. the system is able to replicate the upper stage motion for accelerated mission phases. In the current study, lateral linear first mode sloshing experiments are performed with sinusoidal and impulse sloshing excitation. For each excitation type, natural damping and active damping by closed-loop control is observed. That is, the experiments cover the excited phases, i.e. when the hexapod moves the 1.2 m diameter Perspex tank which is filled with water. After the excitation, natural and active damping occurs and the results are juxtaposed. Note that it was previously shown by Konopka et al. [12] that in the FiPS framework active slosh damping is feasible. However, the current study extends the previous results by experimental data with active slosh damping which was not available before. In Fig. 1 a picture of the experiment during sloshing is shown. The Perspex cylinder is attached to the torispherical bottom made of steel. The tank assembly is mounted atop the hexapod system and sloshing and structure forces are recorded by the force transducers.

Note that water is considered in the current study as an appropriate replacement fluid for liquid hydrogen, liquid oxygen, and liquid methane used in cryogenic tanks since the basic sloshing physics is the same at all fluids. The lower viscosity at cryogenic liquids compared with water does not affect the results at active damping whereas the different densities do affect the force amplitudes. At hydrogen sloshing, the force would be about 14 times lower than at water sloshing which makes force measurement more challenging. Therefore, the current study can be considered to be applicable to all fluids with the only difference being the measurement of the force signal.

The paper is organized as follows. First, the DLR hexapod system is described in detail including the measurement and drive systems. Next, the geometry and mass of the Perspex tank is given which is mounted aboard the hexapod system. Subsequently, the FiPS simulator is introduced including the adaptation to the current hexapod experiments. Furthermore, the Flow-3D model and control algorithm for active sloshing damping which was used in the real-time system at the hexapod is introduced. Next, the sloshing parameters of the experiments and simulations are given and in the results section the experimental results are compared with the FiPS simulations. Finally, some conclusions are drawn.

2. DLR hexapod system

As a particular test equipment to generate excitation, a hexapod system [11] (Fig. 2) is available in the cryogenic laboratory at DLR Bremen. The hexapod system consists of a platform, which can be excited with six degrees of freedom by six independent movable legs. Payloads up to 2.5 tons can be mounted on the hexapod system. The payload can be excited to oscillations between 0 and 10 Hz, the amplitude in each direction in space can be varied in the range of 0.3 m and a maximum acceleration of 0.6 g can be achieved. The platform can

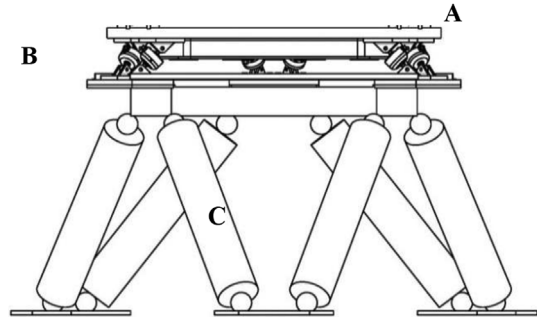


Fig. 2. Hexapod system with experimental platform (A), force transducer (B) and actuators (C).

be tilted to a maximum inclination of 20° while in motion. For mounting the payloads the hexapod system is equipped with an experimental platform. This platform is connected via six struts. Force sensors are integrated into the struts. The prescribed motion and the actively controlled motion of the hexapod system is generated by the real time computer which contains the same control algorithm as the simulation software FiPS.

The resulting force \vec{F}_R on the payload can directly be measured during the test runs by summarizing the data of the six force transducers

$$\vec{0} \equiv \sum_{n=1}^6 \vec{F}_n + \vec{F}_R. \quad (1)$$

In case of liquid sloshing, the resulting force becomes the sum of the liquid force \vec{F}_{liq} and structure force \vec{F}_{str} .

$$\vec{0} \equiv \sum_{n=1}^6 \vec{F}_n + \vec{F}_{liq} + \vec{F}_{str}. \quad (2)$$

The measurement data are processed and recorded by LabVIEW. Each of the force transducer have a relative linearity error of 0.03 %. With a nominal force of 5 kN the nominal error is given as

$$\Delta F_{5kN} = 0.03 \% \cdot 5 \text{ kN} = 1.5 \text{ N}. \quad (3)$$

Finally the resulting error in the excited y-direction can be calculated by summation of the individual errors and dependent on the direction

$$er_{Fy} \equiv \sum_{n=1}^6 \left(\left| \frac{\partial f}{\partial Fy_n} \right| \cdot \Delta F_{5kN} \right) = 4.3 \text{ N}. \quad (4)$$

3. Description of the perspex tank and the mounting plate

In Fig. 3 a sketch of the Perspex tank which was used for the current simulations and experiments is given. The Cassini-shaped tank bottom is made of stainless steel. The Cassini shaped bottom is mounted on the hexapod plate sketched in Fig. 2. The Cassini shape was chosen to have a similar shape compared to launcher tank geometries, but note that the diameter ratio of the bottom dome to the cylinder is often larger in launchers tanks compared with the current configuration. The upper part of the tank is made of transparent Perspex to be able to observe the fluid motion during the tank movement. The dimensions of the tank assembly are given in Fig. 3 and the height of 1800 mm is sufficient to slosh large amounts of liquid to benefit from high force measurements particularly during damping phases. The total weight of the tank assembly including the mounting plate of the hexapod above the force transducers is $m_{structure} = 700 \text{ kg}$.

4. FiPS simulator description

In the current section the standard FiPS simulation environment is

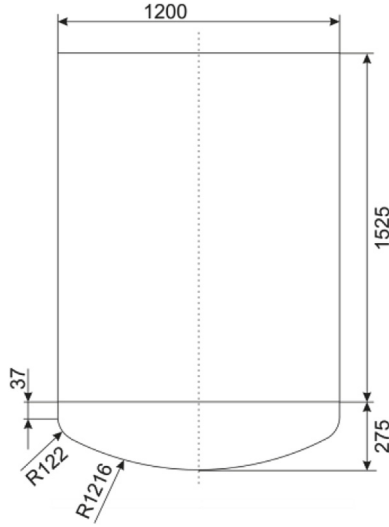


Fig. 3. Perspex tank setup.

described. Furthermore, the stripped-down FiPS version which was used for the current hexapod validation simulations is specified.

4.1. Standard FiPS software

In Fig. 4 a block diagram of the standard FiPS software is given. A detailed description of the simulator is given in Refs. [5], [6]. It is visible that the simulator consists of five main parts.

- The rigid body dynamics [8].
- The flow simulation, i.e. the Flow-3D process modelling the fluid motion. A separate flow simulation is initiated for each tank.
- The thermal modelling of the conduction in the tank structure using ESATAN
- The controller
- The propulsion system

If a stage is equipped with a cold gas reaction control system which is fed by the vapor of the tanks, the propulsion system requires information on the tank pressure and the inflowing liquid or gas density

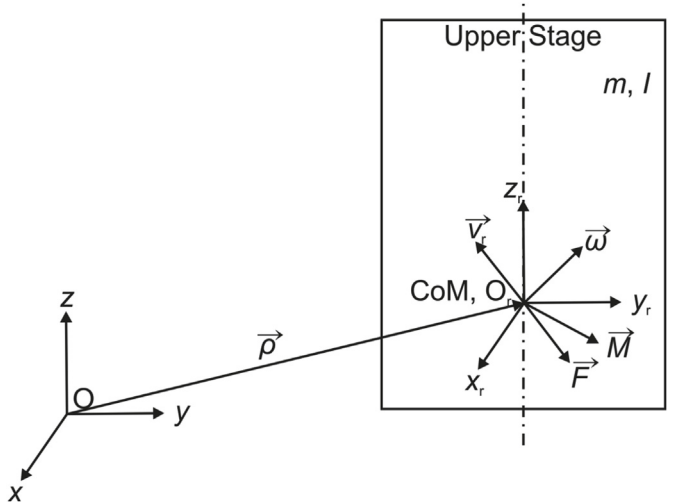


Fig. 5. Sketch of the reference coordinate system and the inertial coordinate system used by FiPS to describe the upper stage motion.

as well as the controller's command to initiate reaction control system (RCS) thruster activations. The command then results in forces and torques, driven by the thrust. The complete set of forces \vec{F} and torques \vec{M} acting on the rigid body are then the sum of RCS forces/torques, the liquid's sloshing forces and torques acting on the tank structure which are computed by Flow-3D as well as external forces/torques, e.g. residual atmospheric drag. The vectors \vec{F} and \vec{M} have their origin in the body-fixed coordinate system as indicated in Fig. 5.

The rigid body's linear acceleration \vec{v}_r , angular velocities $\vec{\omega}$, and mass flow rates at the gas port in the tanks are the boundary conditions for the flow simulations of Flow-3D. The linear \vec{p} and angular momentum \vec{h} equations of the rigid body read [8].

$$\begin{aligned} \vec{p} &= m\vec{v}_r + \mathbf{m}(\vec{\omega} \times \vec{p}) \\ \vec{h} &= m(\vec{p} \times \vec{v}_r) + I\vec{\omega} \end{aligned} \quad (5)$$

Eqn. (5) is written in the inertial reference frame of the spacecraft, i.e. \vec{v}_r is the velocity of the inertial reference frame system and \vec{p} the distance between the origin of the fixed system to the origin of the

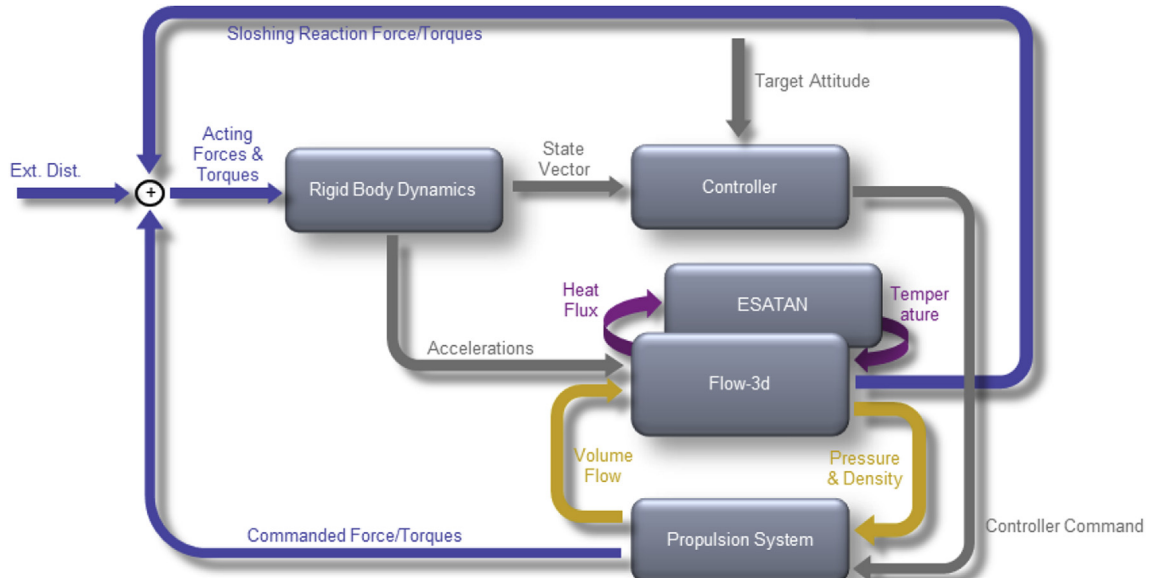


Fig. 4. Block diagram showing the connectivity of the coupled simulation process.

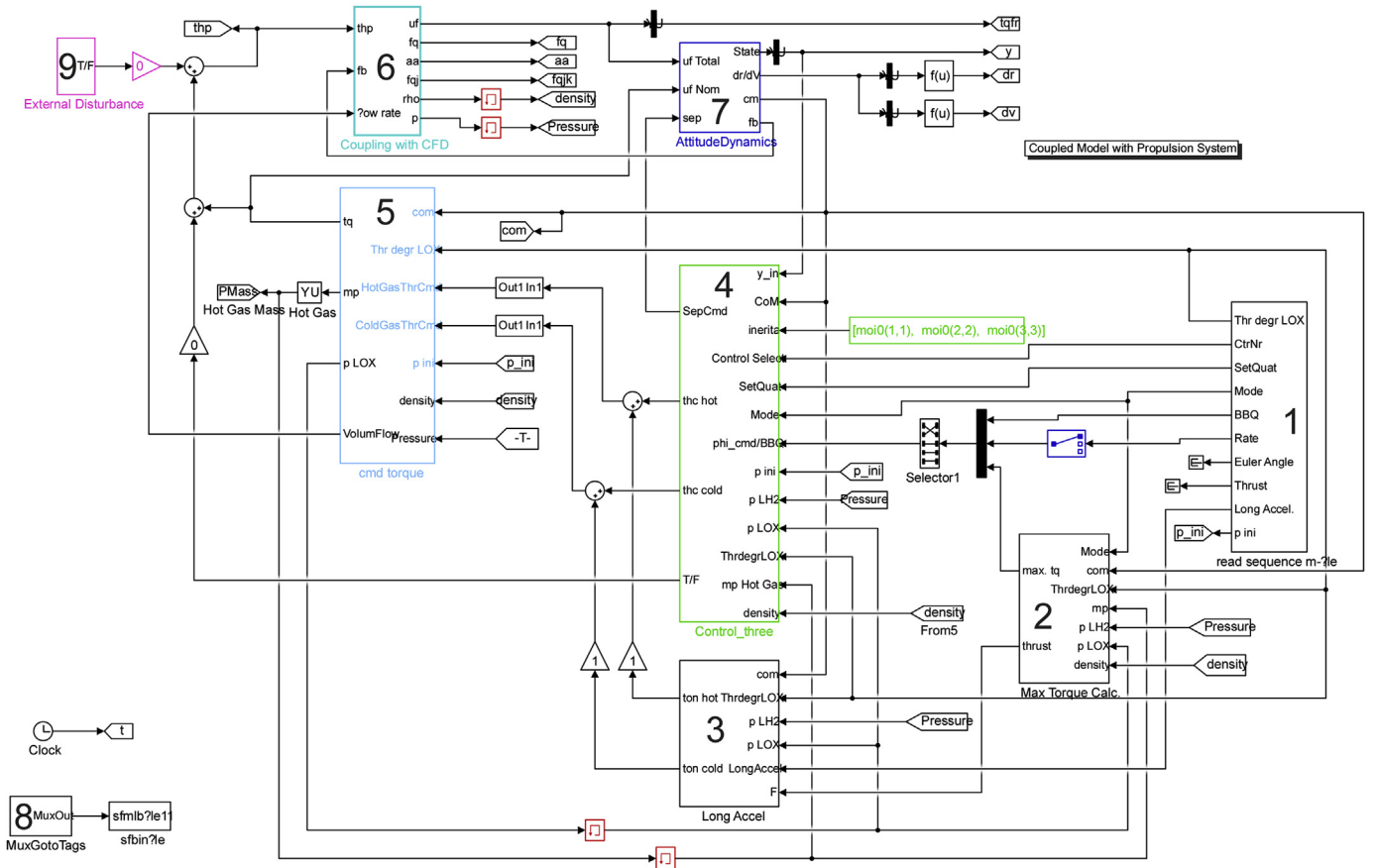


Fig. 6. Matlab®/Simulink® FiPS® simulator model.

inertial reference system which is located at the CoM. The temporal derivation of Eqn. (5) with the inertia tensor I of the rigid body reads

$$\begin{aligned}\vec{p} &= -(\vec{\omega} \times \vec{p}) + \vec{F} \\ \vec{h} &= -(\vec{\omega} \times \vec{h}) + \vec{M}.\end{aligned}\quad (6)$$

The state vector of the rigid body is used by the controller as an input, comparing this value to the target value and initiating new RCS commands, if needed. The heat transfer of the cryogenic liquid to the tank wall occurs at the tank surfaces and is the boundary condition for the solution of the energy equation in the tank walls. For the liquid, the tank wall temperatures are prescribed at each time step and the heat transfer coefficient is computed locally in the fluid.

The simulator is realized in Matlab using the tool boxes provided by Simulink. In Fig. 6 the first layer of the Simulink model is shown. The main blocks of the shown layer are numbered from 1 to 9 simplifying the description of the functionality of the simulator. The blocks of the Simulink model are the following. In block 1 the parameters of the simulation are read. Block 2 serves as an estimator for the maximum forces and torques which are available. Block 3 contains logic for longitudinal thrust generation of the RCS and in block 4 the attitude controller generates RCS commands based on the flight sequence. Block 5 contains the propulsion system and in block 6 the two-way communication routine to Flow-3D is realized. In block 7 the rigid body dynamics [8] is computed based on the internal forces and torques from the flow simulation and external disturbances. Block 8 writes the data to disk for later post processing. Block 9 imposes an external disturbance torque onto the rigid body.

4.2. FiPS adaptation to the hexapod

To utilize FiPS for the present study the Simulink model presented in section 4.1 is simplified preserving the coupling with Flow-3D. Fig. 7 shows the modified Simulink model with three main modules, i.e. the controller block 4 containing the new control logic for lateral sloshing damping, the coupling block 6 where data are exchanged with Flow-3D, and the block 8 where data are sorted for later post processing.

In the framework of the current study FiPS is modified such that the rigid body dynamics [8] (block 7) is removed since the tank is fixed on the hexapod system and cannot drift unconstrained. In the current experiments the force transducers mounted at the hexapod measure the sum of the liquid and structure forces as indicated in equation (2). For the current experiments and simulations the x Cartesian direction is considered, i.e.

$$F_{x\text{Hexapod}} = F_{x\text{Liquid}} + F_{x\text{Structure}}. \quad (7)$$

Therefore, FiPS was modified such that $F_{x\text{Hexapod}}$ is computed in the new block 9 and the information is used by the control algorithm as input data.

$$F_{x\text{Structure}} = m_{\text{Structure}} \dot{x}(t). \quad (8)$$

4.3. Flow-3D model

FiPS relies on Flow-3D to compute the flow in the tanks and to obtain the forces and torques acting on the tank walls. For the current study, Flow-3D version 11.0.4 is used. The governing incompressible Navier-Stokes equations are solved in the liquid phase. The liquid phase is identified in the multiphase flow solver by the volume-of-fluid method [15] and the gas phase is not considered in the current

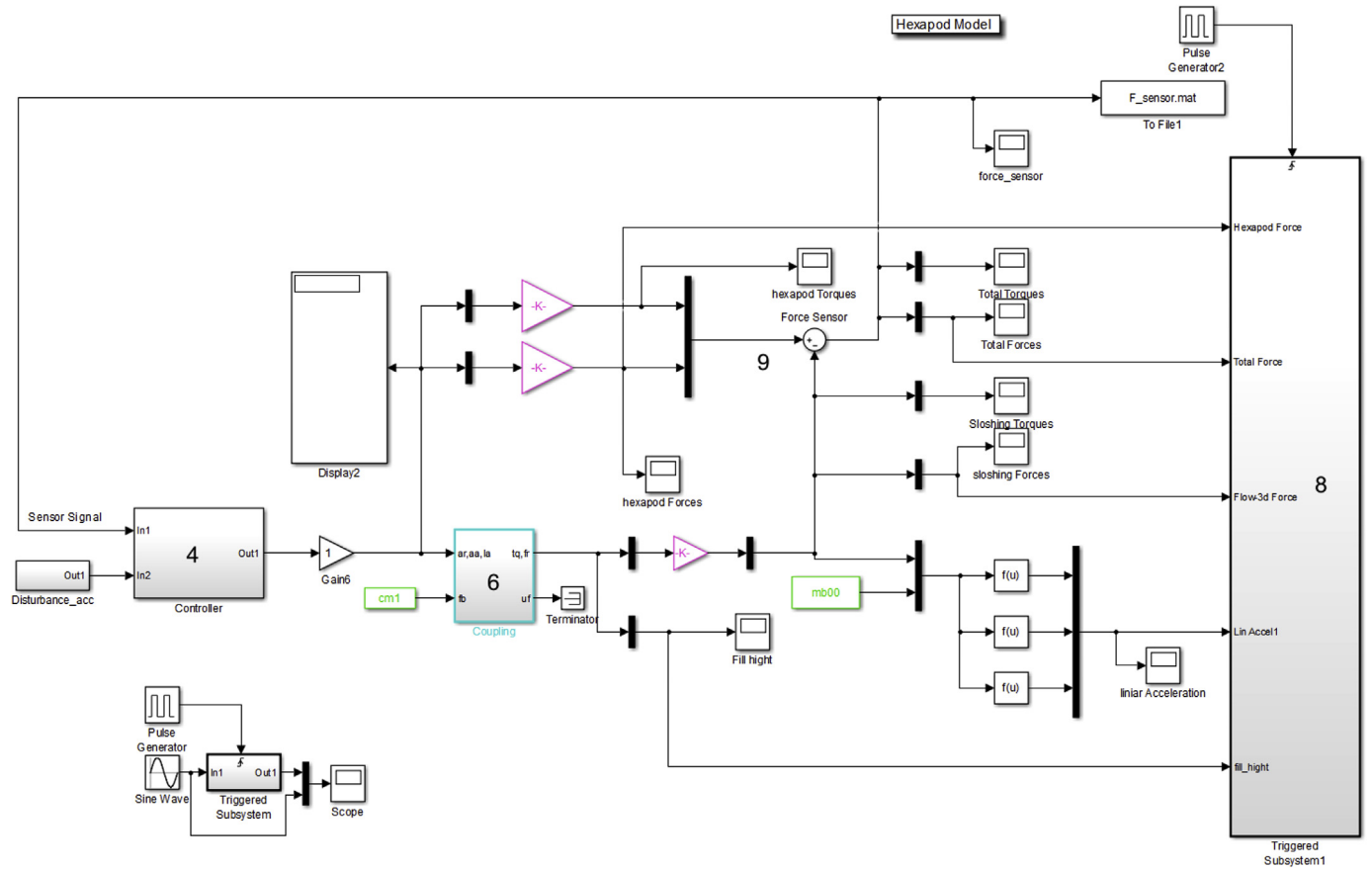


Fig. 7. Matlab®/Simulink® FiPS® Simulator Model update for Hexapod.

Table 1
Fluid properties of water.

Fluid	Viscosity	Density
Water @ 20 °C	$1.01 \cdot 10^{-3} \text{ Pa s}$	997.3 kg/m^3

simulations. The solution of the pressure field is obtained using the generalized minimal residual method (GMRES) [16]. The finite difference methods employed by Flow-3D discretize the governing equations on a Cartesian grid at second order accuracy both for the inviscid and viscous terms. For the current iso-thermal computations the transport properties of water are assumed to be constant and are given in Table 1. The current unsteady, time-accurate flow computation is assumed to be laminar.

In Fig. 8 the Flow-3D model of the Perspex tank the geometry of which was described in section 3 is given. The tank is modeled using the obstacle method, i.e. Flow-3D introduces a volume fraction and face fraction field with blocked and open grid cells which represent the tank structure and fluid domain [9]. That is, the tank wall is modeled by an immersed boundary method which cuts the grid cells. At the tank wall no-slip conditions are enforced. The origin of the Flow-3D coordinate system which is sketched in Fig. 8 is at the lower bottom of the tank. The hexapod coordinate system is located $\Delta z = 329 \text{ mm}$ below the origin of the Flow-3D coordinate system. The initial condition of the simulations is that the tank is filled with water at 0° surface inclination at different fill levels which are indicated in Table 4.

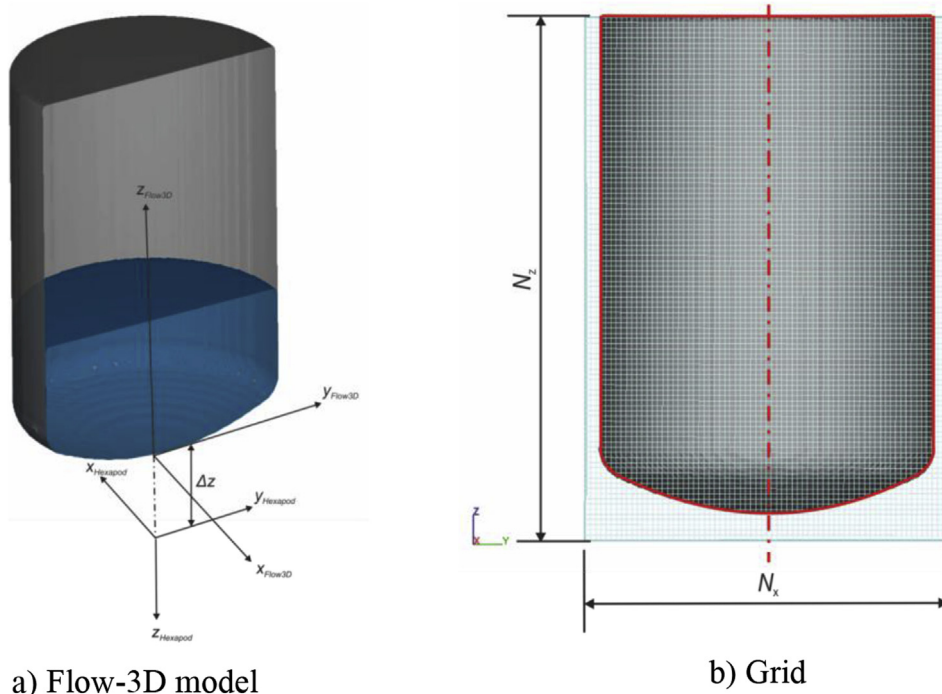
The current simulations are performed on two grids the parameters of which are given in Table 2. The grid study which was performed in the results section indicated that the resolution at grid two is sufficient to match the experimental force evolution.

4.4. Control algorithm

Propellant sloshing in space vehicles can pose different problems. It may cause instability of the closed loop system, excessive consumption in the attitude propellant or problems for engine re-ignition. Up to now the way to actively address these issues is only by design measures in the tank layout. On the algorithm side the instability problem is addressed by gain or phase stabilization via notch filters, which may be regarded as only passive. To our knowledge, no means of actively influencing the sloshing phenomenon is currently employed. The controller which has been developed in the framework of the FLPP3 program [10] is a first step towards an active handling of sloshing by increasing the knowledge concerning modelling and control design and by testing closed loop methods via experiments.

In order to be successful, various techniques must be mastered covering modelling, control design, and implementation into an embedded test system. A new element is that the sloshing has to be adequately modeled for the controller design task. Such a model is not necessarily identical to a very precise computational fluid dynamics (CFD) based model as commonly used for prediction. This activity is also a step in the validation of the CFD modelling as far as closed loop prediction is concerned. Usually the validation between CFD simulation and actual tank sloshing is done in open loop by applying, for a certain period, an excitation (forced motion) which is followed by stopping the excitation and then observing the damping. In the closed loop scenario a different pattern of excitation will be generated which is more realistic. Therefore, this kind of test will give additional insight concerning the validation of the CFD prediction capability.

Fig. 9 illustrates the workflow from control design based on a spring/damper model via physical modelling of the hexapod and Flow-3D in the loop toward the final test with embedded controller



a) Flow-3D model

b) Grid

Fig. 8. Flow-3D model of the Perspex tank showing the origins of the Flow-3D coordinate system in the center of the tank and the hexapod coordinate system which is located in the mounting plate below the tank a) and discretized Perspex cylinder with a Cartesian grid b).

Table 2

Grid parameters for grids 1 and 2.

Grid	Number of cells	Minimal grid spacing
1	$N_x \cdot N_y \cdot N_z = 70 \cdot 70 \cdot 101 = 494900$	$\Delta x \cdot \Delta z \cdot \Delta z = 1.82 \text{ cm} \cdot 1.82 \text{ cm} \cdot 1.82 \text{ cm}$
2	$N_x \cdot N_y \cdot N_z = 140 \cdot 140 \cdot 203 = 3978800$	$\Delta x \cdot \Delta z \cdot \Delta z = 0.92 \text{ cm} \cdot 0.92 \text{ cm} \cdot 0.92 \text{ cm}$

implemented in the hexapod test environment of the hexapod system.

A CFD model is useful for prediction of the sloshing motion, but it is not immediately useful as a controller design model. In the new model based design methods the resulting controller structure is in part

determined by the choice of the design model. The purpose of the current activity is that the whole chain composed of the two models (CFD and controller design), the design method and the validation on a hexapod is mastered.

Fig. 10 shows a sketch of the design model for the current control algorithm. The hexapod system generates the external force $F_{x\text{Hexapod}}$ which is measured by the force transducers given in section 2 and is used for control. The liquid force F_{liquid} is used for providing the input for the performance weightings needed in the controller design. The sloshing masses for the current tank and fill levels were derived numerically using potential theory [3] [4], and a geometrical model of the tank. The computed sloshing mass m_s , the rigid liquid mass + structure

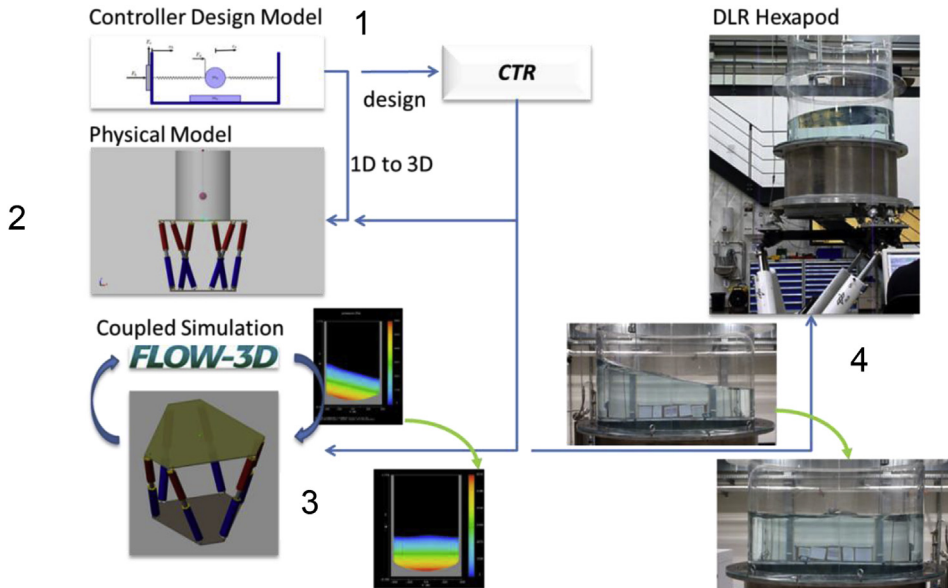


Fig. 9. Workflow: Design and Test: 1) Controller design based on mathematical model 2) Controller test with physical model of the hexapod (Simmechanics) 3) Extension of the physical modelling with Flow-3D 4) Test on hexapod.

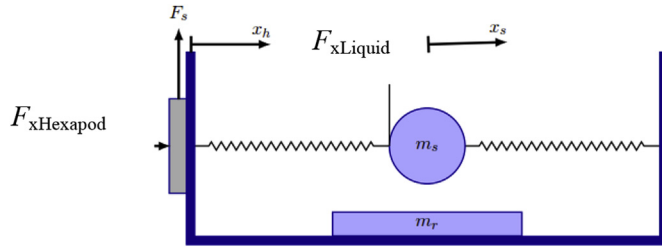


Fig. 10. Controller design model: Point mass representing the slosh mass m_s attached in a movable frame with mass m_r (comprising the mass of the frame $m_{\text{structure}}$ as well as the non-sloshing mass of the fluid) with a spring/damper system. (The damping is omitted in the picture).

Table 3
Computed parameters of the spring-damper model.

Case	m_s	m_r (rigid liquid mass + structure mass)	c
1,2	291 kg	335 kg + 700 kg	8286.1 N/m
3,4	307 kg	958 kg + 700 kg	9251 N/m

mass m_r , and the spring constant are given in [Table 3](#). Note that only the first sloshing mode is considered. The current spring-damper or the equivalent pendulum model are limited to small sloshing angles, i.e. $< 15^\circ$. Models which are valid for higher sloshing angles are available, see e.g. Ref. [18]. However, since a robust controller is derived by model-based design, large sloshing angles can be handled even if the underlying spring-damper model is limited to sloshing angles $< 15^\circ$.

The set of differential equation of the system as depicted in [Fig. 10](#) can be derived following basic rules of mechanics. The details are reported in Ref. [11]. The core feature of the concept is the use of a force sensor which provides information on the fluid motion via the detected reaction force. The controller uses as a feedback this force measurement. When properly taking into account the reaction force from the structure which is created by the controller's own commands, the remaining force contains the information of the fluid. Commands can then be generated which will damp the motion.

Konopka et al. [12] evidenced that the match between controller design model (see [Fig. 10](#)) and the CFD model is convincing at least in an open loop condition for linear lateral sloshing. However, it is still necessary to build sufficient robustness into the controller in order to deal with uncertainties in the real fluid as well as in the un-modeled effects in the actuation chain of the Hexapod. Therefore a robust control design is needed in order to deal with expected and un-expected uncertainties. The design and analysis is based on structured singular value theory [17]. The linear fractional transformation model is shown

in [Fig. 11](#). The inputs of the model are the measurement noise n and the disturbance F_d . Note that for a space application the sloshing force cannot be directly measured and the controller input would have to be changed with longitudinal acceleration which can be measured by the inertial measurement unit. The outputs of the model are the relative velocity p and the control effort e . The controller input/output (blue) are the commanded hexapod acceleration \ddot{x}_{cmd} and the force measurement F_{xHexapod} . Further elements of the model are the LP_x low pass modelling hexapod drive and force sensor elements and the differential equation DEQ representing the system from [Fig. 10](#).

A structured-uncertainty μ -synthesis controller has then been computed based on the modelling. The design was tested with a hexapod model established in the commercial modeler Simmechanics as shown in [Fig. 12](#). This environment allows the user to select either design model, hexapod with pendulum or, with some addition for the FIPS interface (see [Fig. 7](#)), CFD in the loop.

4.5. Sloshing and control parameters

The current sloshing experiments and simulations are performed at normal gravity with two different sloshing excitations, i.e. with impulse excitation and with a sinusoidal excitation. The parameters of the excitations are given in [Table 4](#). For the sinusoidal excitations at cases 3 and 4, the linear acceleration in the Cartesian x-direction is given by

$$\ddot{x}(t) = -\omega_c^2 x_a \sin(\omega_c t). \quad (9)$$

Each of the experiments and simulations at cases 1 and 3 without control are divided into an excited phase where the hexapod moves and a natural damping phase where the hexapod rests where natural damping is observed. Cases 2 and 4 are divided into three phases each, i.e. an excited phase where the hexapod moves and the sloshing motion is initiated, a natural damping phase where the hexapods rests and an active damping phase where the controller commands hexapod movements based on the force measurements to actively damp the sloshing motion. The excitation parameters at cases 3 and 4 are chosen such that the excitation frequency is below the resonance frequency of the tank of 0.87 Hz at both fill levels [3], [4]. Two fill levels were chosen at cases 1–4 since at different fill levels the sloshing properties of the liquid such as the ratio of slosh mass to rigid mass differs. Therefore, at cases 2 and 4 a different set of control parameters is used in the experiment and in the simulator.

5. Results

The results section is split into the discussion of the results of the open and closed loop experiments and simulations for the lower fill level of 635 mm at cases 1 and 2 and for the higher fill levels of 1200 mm at cases 3 and 4.

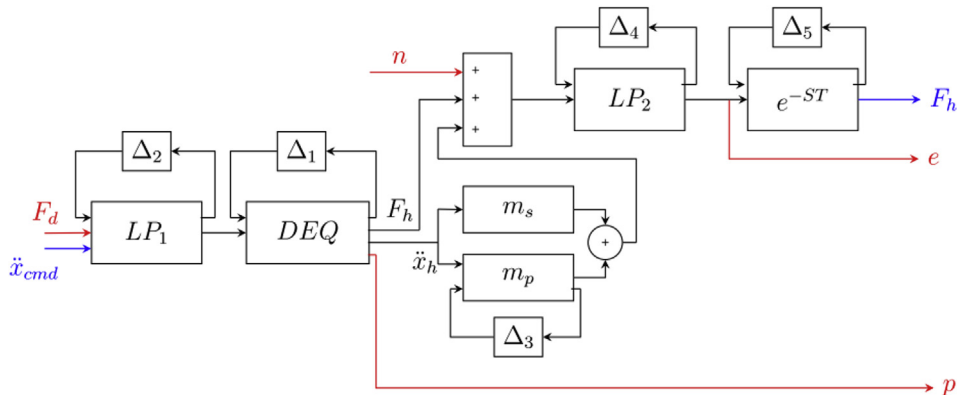


Fig. 11. Linear Fractional Transformation (LFT) model with input/output for performance weighting (red). (For interpretation of the references to colour in this figure legend, the reader is referred to the Web version of this article.)

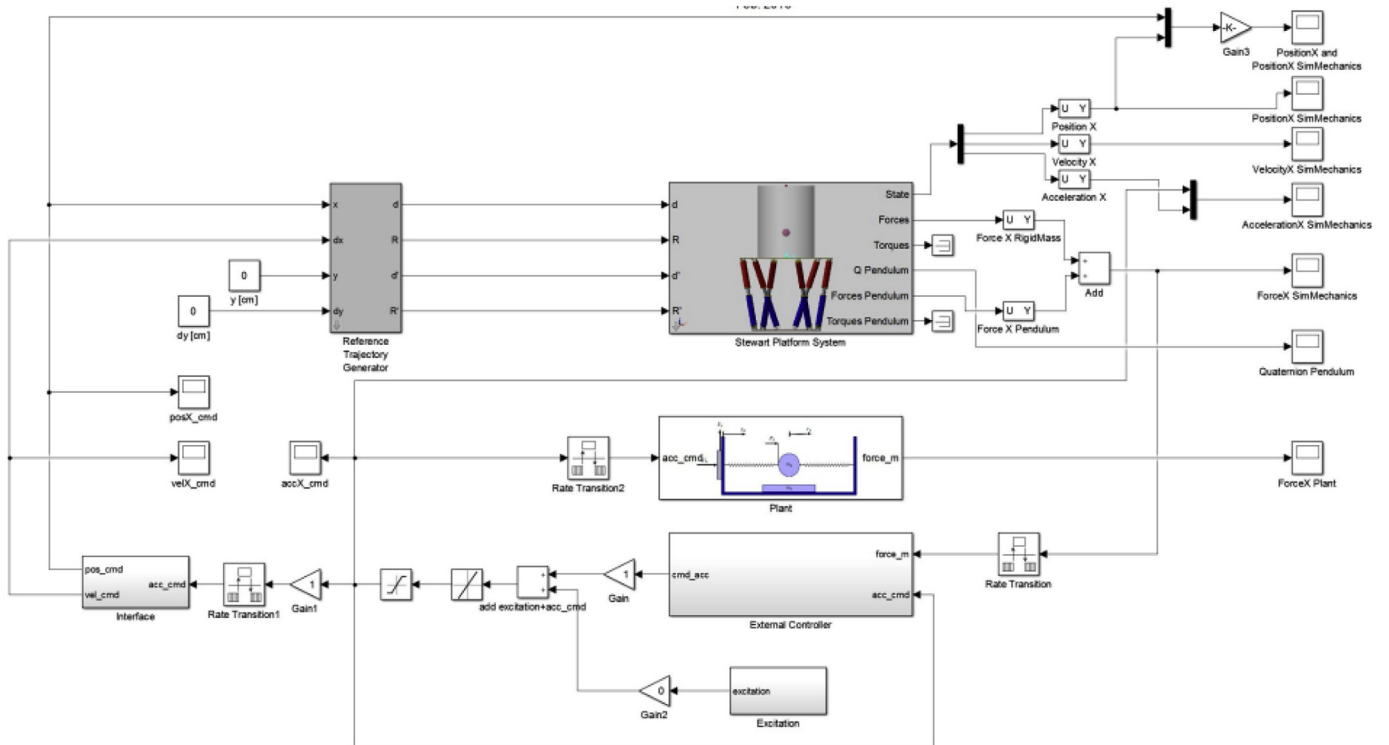


Fig. 12. Physical modelling environment with options for design model or Simmechanics hexapod in the loop.

Table 4

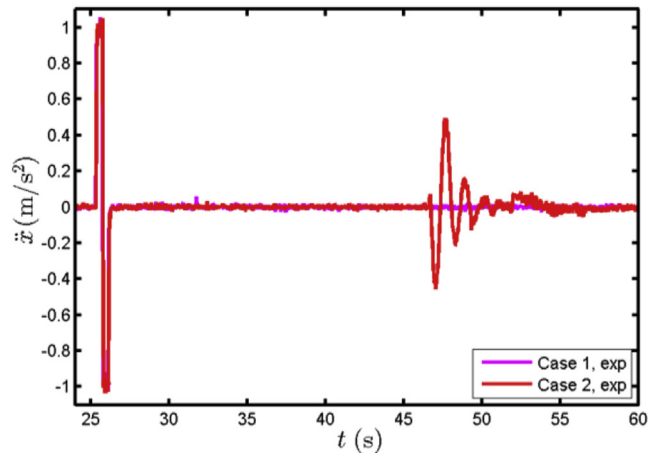
Parameters of the current simulations and experiments.

Case	Excitation Frequency f_c	Excitation Amplitude x_a	Excitation maximum acceleration \ddot{x}_{max}	Control loop	Fill level	Method
1	–	–	1 m/s ²	open	635 mm	Experiment, FiPS
2	–	–	1 m/s ²	closed	635 mm	Experiment, FiPS
3	0.74 Hz	20 mm	0.43 m/s ²	open	1200 mm	Experiment, FiPS
4	0.74 Hz	20 mm	0.43 m/s ²	closed	1200 mm	Experiment, FiPS

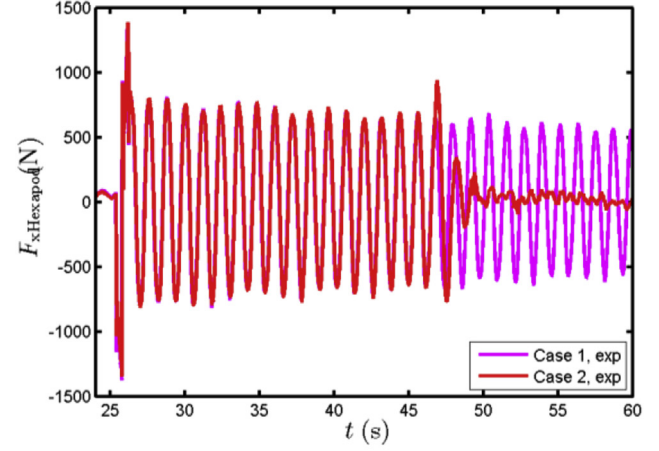
5.1. 635 mm fill level (cases 1 and 2)

In Fig. 13 a) the measured acceleration of the DLR hexapod system in the x -axis direction is given for cases 1 and 2, i.e. for the open and closed loop sloshing cases. It is visible that at $t \approx 26$ s the hexapod accelerates to the target acceleration of 1 m/s^2 and subsequently

decelerates to reach a zero velocity and after that the acceleration remains zero. At case 2 the same excitation pulse is used but at $t \approx 47$ s the controller commands lateral excitations to actively damp the sloshing motion. The corresponding force evolutions are shown in Fig. 13 b). It is visible that the total hexapod force is about 1.4 kN during the excitation pulse at $t \approx 26$ s. Afterwards, lateral linear



a) Acceleration



b) Force

Fig. 13. Juxtaposition of the open and closed loop experiments at cases 1 (open loop) and 2 (closed loop) for the fill level of 635 mm.

Table 5
Computed damping ratio γ

Case	Phase	Experiment	Experiment standard deviation	Damping ratio γ_1/γ_n
1	Natural Damping	0.0021	0.00034	1
2	Natural Damping	0.0019	0.00023	1.123
2	Active damping	0.11	0.0037	53

sloshing at the first mode occurs which leads to a sinusoidal force evolution with a natural frequency of $f = 0.872$ Hz [3], [4]. At $t \approx 47$ s the control algorithm kicks in and the sloshing motion is actively damped, i.e. the force amplitude is reduced from ± 650 N to about ± 80 N demonstrating that the closed-loop system is able to damp the sloshing motion within two cycles.

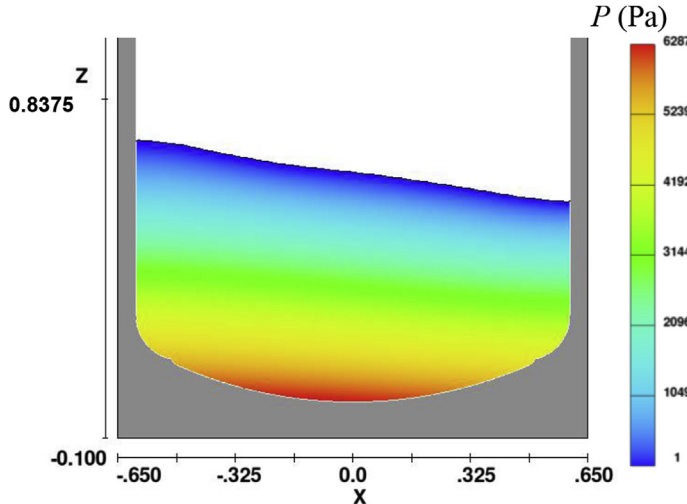
The damping of the liquid is further characterized by the damping ratio γ which is computed from the logarithmic decrement Λ of the liquid force by Ref. [3].

$$\gamma = \frac{\Lambda}{2\pi} = \frac{1}{2\pi} \cdot \frac{1}{i} (\ln F_0 - \ln F_i), \quad (10)$$

where F_0 is the first force amplitude in the damping phase and F_i the i -th force amplitude. In the current evaluation of γ up to 40 force peaks are considered and γ is determined by a least-squares method. In Table 5 the damping ratios of the experiment of the natural damping which occurs in the Perspex tank at cases 1 and 2 are given. At case 2, the damping factor γ for the natural damping phase before active sloshing reduction is computed by only 15 amplitude peaks vs. 40 peaks for case 1, explaining the difference. At active damping at case 2, the damping ratio is about 53 times higher than at case 1. However, the damping ratio at the active damping phase at case 2 can only serve as a rough estimate since it is based on four force peaks and the damping ratio is valid for non-actuated systems at the natural sloshing frequency.

In Fig. 14 the surface inclination at $t = 28$ s during the excitation peak at case 1 is shown for both the simulation and the experiment. It is visible that a smooth surface occurs both in the simulation and experiment and that the first lateral sloshing mode is excited.

In the current study two grids are used and both grids 1 and 2 predict the maximum amplitudes with an accuracy of 7%. However, the finer grid 2 better predicts the natural sloshing frequency which is



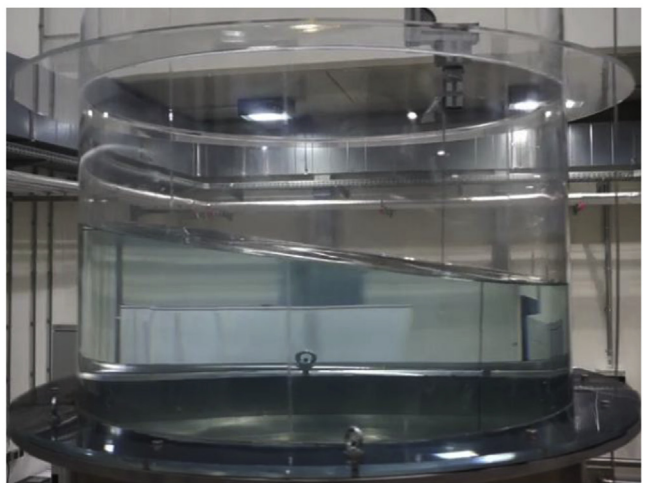
a) Case 1, grid 2, $t = 28$ s, x - z -plane

visible in Fig. 15 a). Therefore, all subsequent computations were performed with the finer grid 2. In Fig. 15 b) the hexapod force evolutions of the experiment and the simulation at case 1 are juxtaposed. It is visible that the data matches, indicating the quality of both the experiment and the simulation.

Fig. 16 a) shows the hexapod acceleration at the simulation at case 2 and the experiment at case 2 during active damping. It is visible that movement of the hexapod starts at $t \approx 47$ s. There seems to be a large difference between simulation and experiment right at the start of the damping phase in the acceleration plot. The controller module aims to start the commands at the moment of the zero crossing of the force measurement. In principal the damping controller will work independently of the instant of start, but by this special timing the hexapod stroke is minimized and stays within its limit. However, when there are slight differences in the zero-crossing detection (order of 10 ms) the commanded acceleration from the controller are different at the beginning. This happened in the simulation where the green curve starts earlier than the red. Yet, the subsequent damping performance is not effected and a convincing agreement between simulation and experiment is achieved. In Fig. 16 b) the hexapod force evolution of the simulation and the experiment is juxtaposed. It is evident that the simulated force evolution closely follows the experiment and lateral sloshing is damped within two cycles. This indicates the correctness of the data exchange between controller, simplified rigid body dynamics, and Flow-3D simulation.

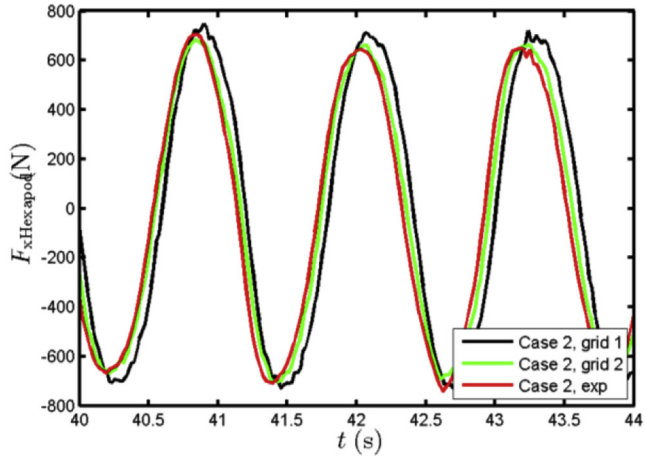
At $t \approx 47$ s the force increases when hexapod movements are commanded and the structure force adds to the liquid force. Therefore, the liquid force evolutions in the experiment and the simulation at case 2 are juxtaposed in Fig. 17. It is visible that there is no liquid force increase during the active damping period $46.5 \leq t \leq 51$ s and the controller commands always lead to a sloshing force reduction.

Fig. 18 shows the liquid positions at cases 1 and 2 both in the simulation and in the experiment. The numerical liquid position in the x - z plane are shown in Fig. 18 a) and b) at the natural damping case 1 and the active damping case 2. It is visible that the large lateral damping motion has been eliminated and only some irregular surface waves remain. The fluid position in the simulation at case 2 at $t = 52$ s after active damping is completed corresponds to the image of the experiment shown in Fig. 18 c) where some residual surface waves are visible. The remaining irregular surface motion explains the residual force which is present after active damping.

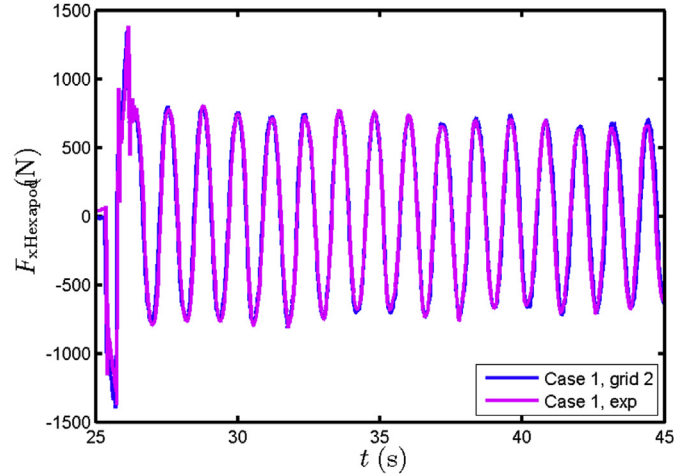


b) Case 1, exp, $t \approx 28$ s

Fig. 14. Maximum surface excitation during the impulse excitation at case 1.

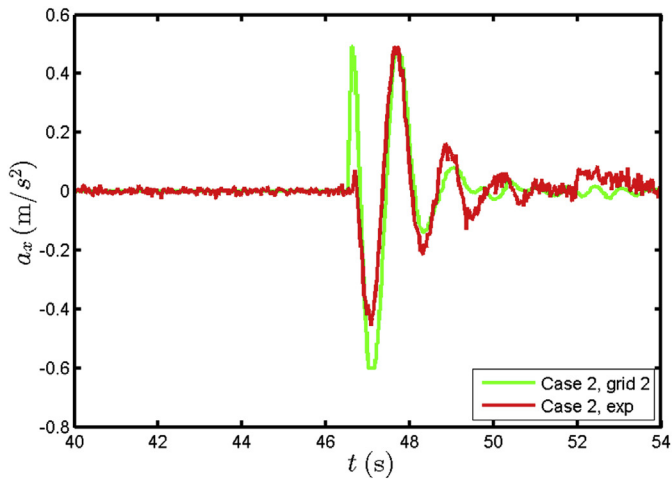


a) Grid study at case 2

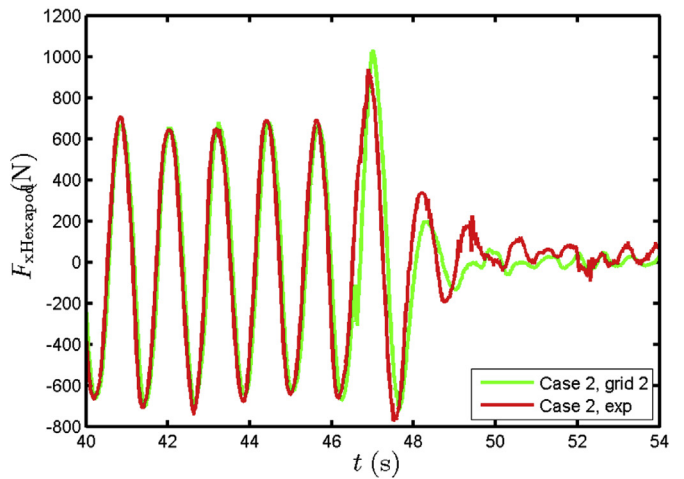


b) Juxtaposed hexapod force evolutions at case 1

Fig. 15. Juxtaposed hexapod force evolutions for cases 1 and 2.



a) Acceleration



b) Force

Fig. 16. Acceleration and hexapod force evolution of the active damping case 2, experiment and simulation at grid 2.

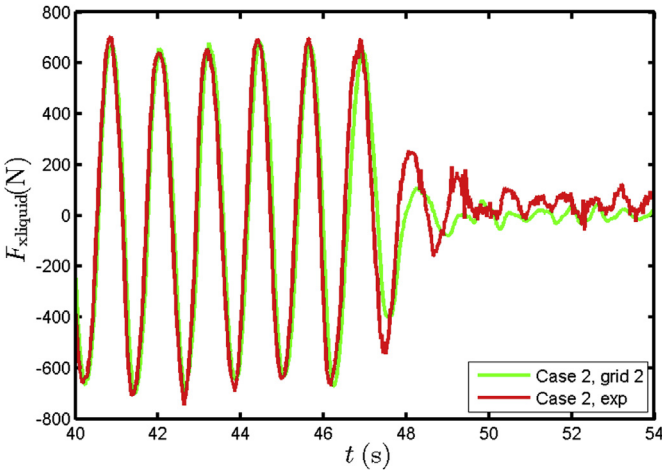


Fig. 17. Comparison of the numerically obtained liquid force evolution in FiPS and the liquid force deduced from hexapod force and acceleration measurements by eqn. (7).

5.2. 1200 mm fill level (cases 3 and 4)

In the current section the numerical results of the FiPS/Flow-3D simulations are compared with the measurements at cases 3 and 4 for the higher fill level of 1200 mm and a sinusoidal excitation. In Fig. 19 the measured acceleration and the force evolutions at case 4 are compared. It is visible that during the excited phase at $t \leq 272$ s the measured acceleration and hexapod force evolutions of both cases match indicating the repeatability of the experiment. Active damping occurs at $t \approx 293$ s and it is visible in Fig. 19 b) that a nearly complete force reduction is reached by the control commands within two sloshing cycles. That is, the controller with the updated parameters for the higher fill level remains highly effective and robust.

In Table 6 the damping ratios γ for experiments at cases 3 and 4 are given. The reason for the difference of the damping ratio γ for the natural damping phase is that only about 15 cycles for the damping computation of case 4 vs. 40 cycles at case 3 are considered. When the sampling window at case 3 is reduced to 15 cycles, the same damping ratio is obtained as at case 4. During active damping four force peaks are used to determine the damping ratio γ which is 113 times higher than at natural viscous damping indicating the quality of the control algorithm.

In Fig. 20 the surface inclination before the end of the sinusoidal

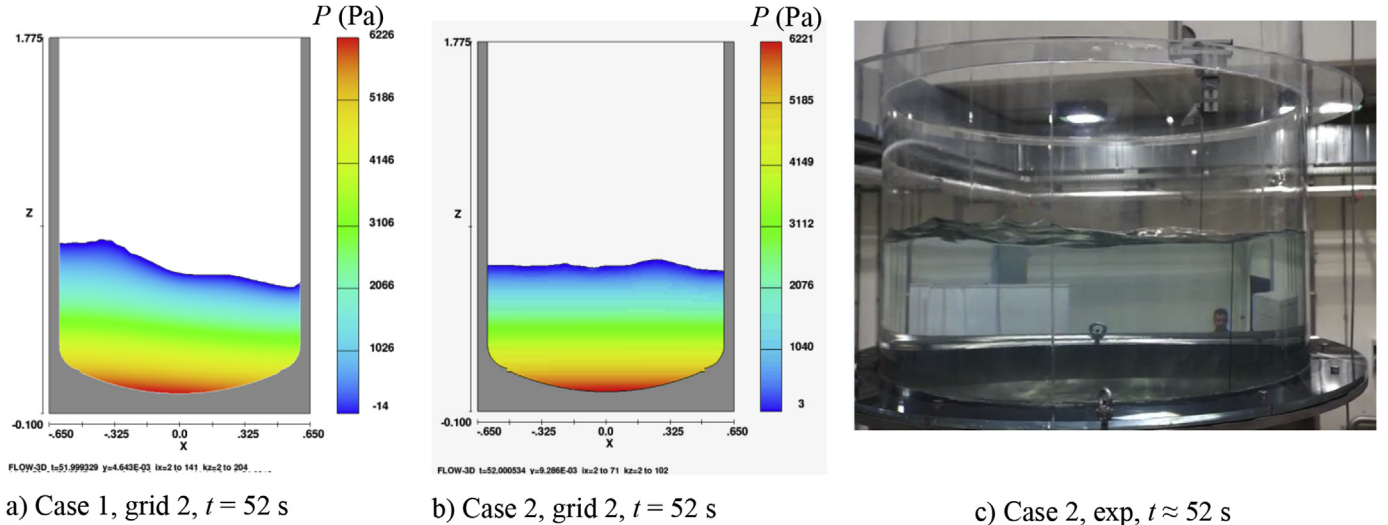


Fig. 18. Fluid pressure contours of the natural damping and active damping simulations at cases 1 and 2 and image of the surface shape of the experiment at case 2.

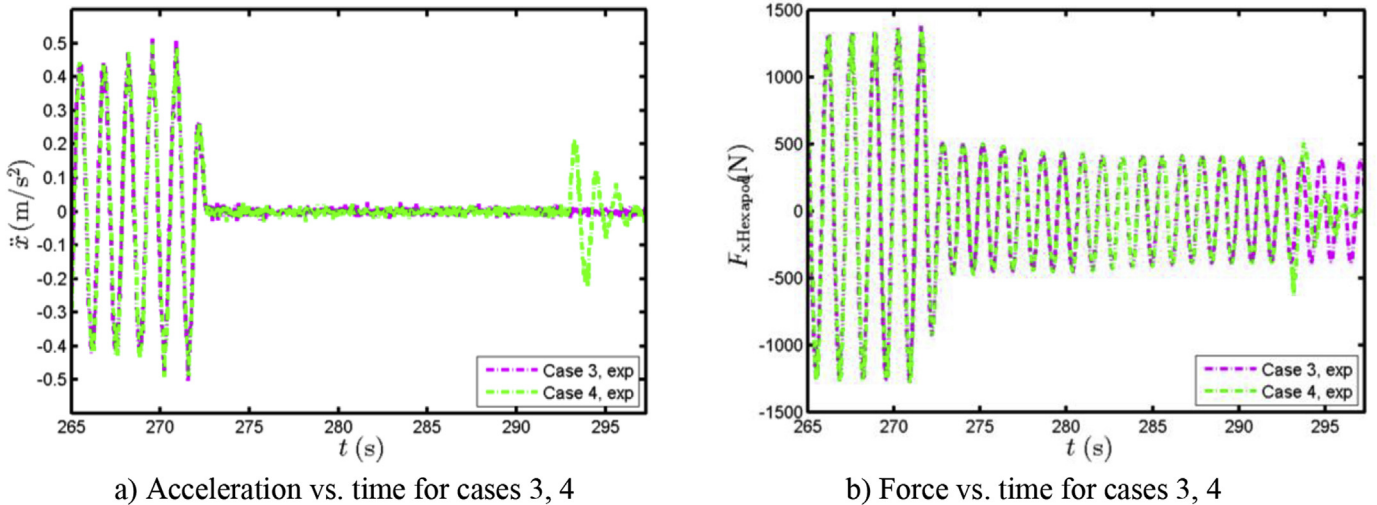


Fig. 19. Juxtaposition of the open and closed loop experiments at cases 3 and 4 for the fill level of 1200 mm.

Table 6
Computed damping ratio γ

Case	Phase	Experiment	Experiment standard deviation	Damping ratio γ_3/γ_n
3	Natural Damping	0.0011	0.000030	1
4	Natural Damping	0.0021	0.00020	0.5
4	Active damping	0.12	0.0011	113

excitation at case 3 is shown in a x - z -plane for the simulation and in the image for the experiment. It is visible that first mode linear lateral sloshing occurs with a smooth liquid surface.

The grid study at the higher fill level case 3 which is given in Fig. 21 a) shows that at grid 2 the simulation data indicates a convincing agreement with the simulation data since the natural sloshing frequency [3] of $f = 0.872$ Hz is matched. In Fig. 21 b) the hexapod force evolution of case 3 of the FiPS simulation is compared with the experiment at case 3 at the time when the hexapod excitation is switched off at $t \approx 272$ s. It is evident that a convincing agreement both during excitation and natural damping phases occur.

In Fig. 22 a) the measured hexapod acceleration evolution at case 4 is compared with the simulation using grid 2. It is visible that the controller in the simulator commands slightly higher acceleration levels than those which occur in the experiment. The reason for the discrepancy is that the FiPS simulation environment uses a simplified hexapod model which is approximated as a point mass. However, the simulation at case 4 matches the frequency of the sloshing motion during damping at $293 s \leq t \leq 297$ s. The hexapod force evolution in Fig. 22 b) shows that in the simulation the initial force amplitude during active damping at $t = 294$ s is overpredicted by about 24% which is due to the higher acceleration which is commanded by the control algorithm in the simulator. The subsequent force cycles are closely matched in frequency with slightly higher force amplitudes occurring in the simulation. The qualitatively good match shows that at the higher fill level case 4 the information data transfer between Flow-3D, simplified rigid body dynamics, and control algorithm is correctly implemented and the sloshing dynamics with and without control is accurately captured.

The liquid force evolution at the simulation and at the experiment at case 4 is juxtaposed in Fig. 23. It is visible that in the experiment the liquid force decays at $t \geq 293.5$ s when active damping is initiated. In the simulation, the controller produces a slight liquid force increase which is subsequently quickly damped by controller action. That is,

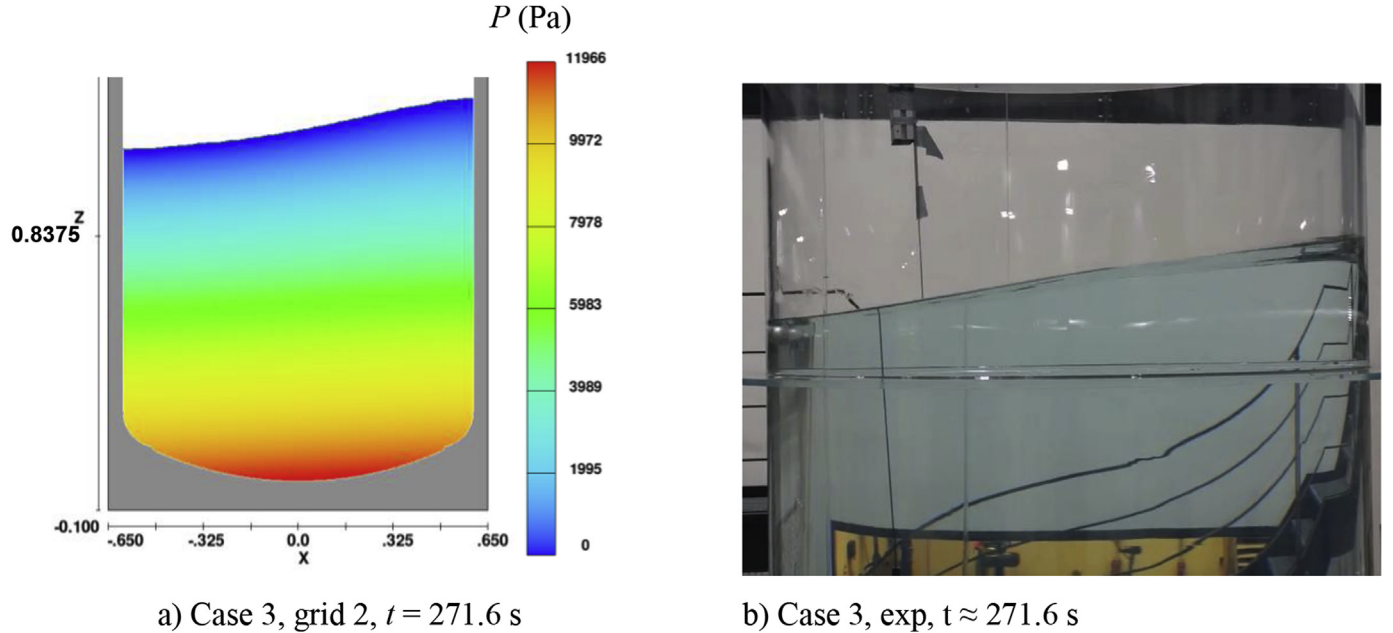


Fig. 20. Surface inclination at the end of the excitation period at case 3 at the simulation and experiment.

despite some discrepancies for the force peaks the controller behavior is similar in the FiPS simulation environment and in the real-time system of the hexapod.

In Fig. 24a) and b) the liquid surface position in x - z -planes at $y = 0$ is compared for the natural damping case 3 and the active damping case 4. It is visible that the controller has effectively damped the sloshing motion and the liquid surface is nearly flat. The same holds for the liquid surface of the experiment at the same time $t = 295$ s at case 4 at which the sloshing motion has been effectively damped by the controller and the hexapod movement.

6. Conclusion

First mode water sloshing was investigated both in an experiment and in a simulation environment. In the experiment, a 1.2 m diameter Perspex tank was mounted aboard the DLR Hexapod system in the Cryo-Lab at the Institute of Space Systems in Bremen. The hexapod system was replicated as a point mass in the FiPS simulation environment. The FiPS simulation environment couples the rigid body

dynamics of the hexapod system, the control algorithm and the sloshing dynamics of the water tanks. The flow computations within FiPS were performed using the commercial flow solver Flow-3D. The purpose of the study was to show that active damping of sloshing water in a large vessel is possible by having a controller in the real-time loop of the hexapod system and that FiPS can rebuild these experiments with a high accuracy.

To do so, four test cases were considered with two fill levels. At the lower fill level of 635 mm open and closed loop sloshing experiments with an impulse excitation were performed and it was shown that the control algorithm is able to damp the linear lateral sloshing in two cycles within 4 s. The experiments evidence that the controller produces a damping factor which is 53 times higher than at natural viscous damping. The FiPS simulations were accurate within 5% with respect to the sloshing force during natural damping and during active damping in closed-loop control the damping period show very good agreement with an accuracy of 4%. At the higher fill level of 1200 mm the set of open and closed-loop experiments was repeated. The FiPS simulation force data collapses with the measurements during excited and non-excited

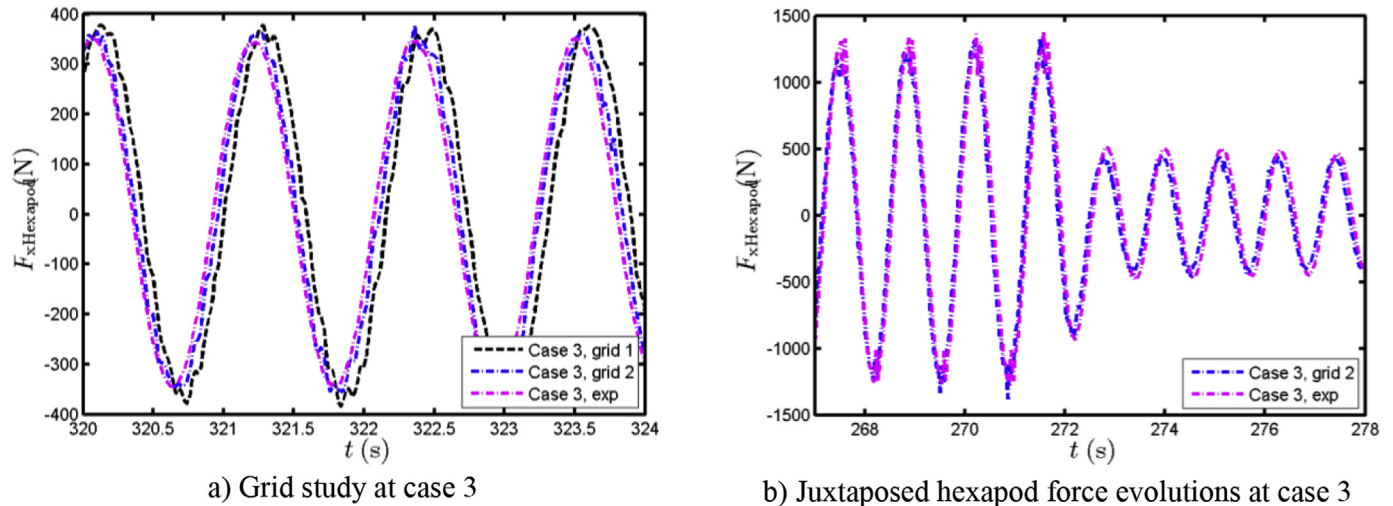
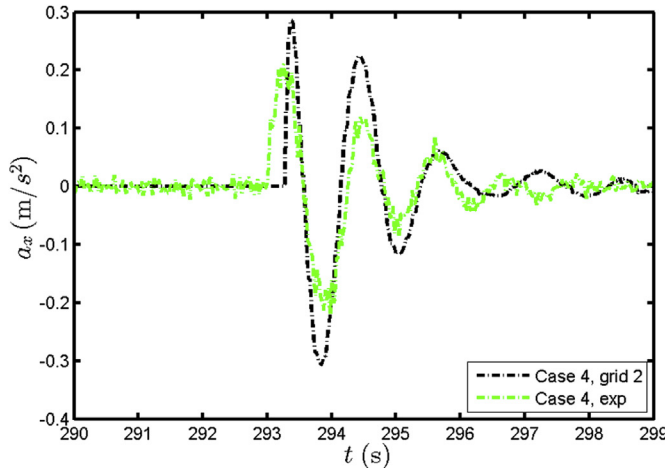
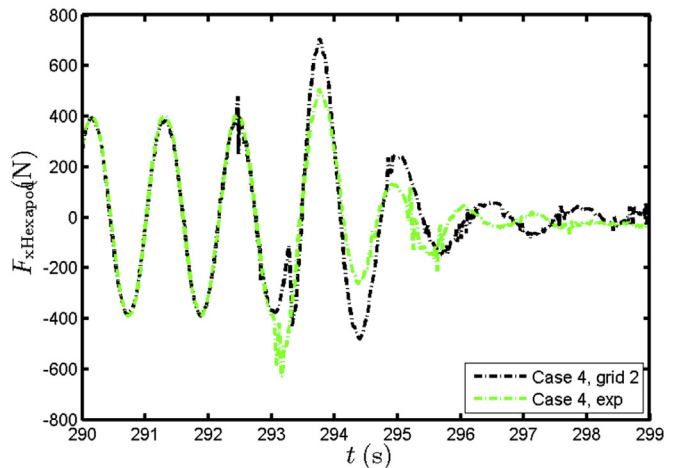


Fig. 21. Juxtaposed hexapod force evolutions at case 3.



a) Acceleration



b) Hexapod force

Fig. 22. Acceleration and hexapod force evolution of the active damping case 4, experiment and simulation at grid 2.

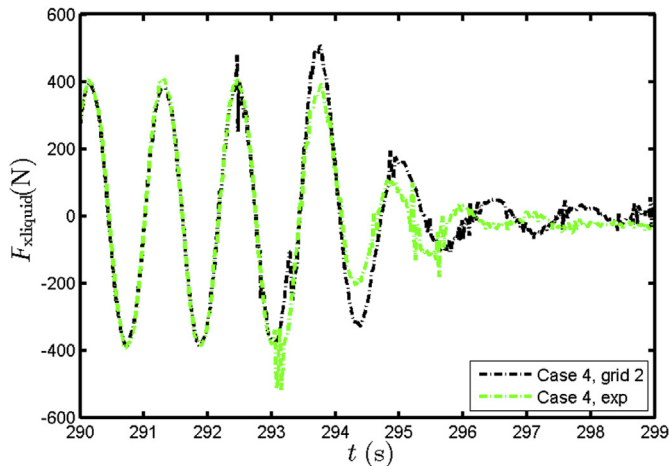


Fig. 23. Comparison of the liquid force evolution of the simulation and of the experiment at case 4.

phases of the sloshing motion. At active damping, the simulations match the damping period and the hexapod forces with an accuracy of 20%.

The conclusion is that the model-based control algorithm is able to damp lateral linear sloshing within two sloshing cycles at different fill levels. Furthermore, the FiPS simulation environment is validated for

sloshing phases with external excitation, during natural damping, and at active close-loop sloshing control. The current on-ground experiments are similar to in-orbit maneuvers such as propellant settling with a low longitudinal acceleration and as such the current validation also extends to orbital phases. However, other coupled phenomena such as an upper stage in spin mode with sloshing propellants in the tanks require low gravity experiments for validation which will be pursued in a second step of the FiPS validation effort.

The current experiments and simulations demonstrate that active sloshing control is a viable option for future upper stages such as that for Ariane 6 and that the currently used FiPS simulation environment is well validated for coupled sloshing simulations and the application to accelerated mission phases.

Acknowledgments

A part of the work has been performed in the context of ESA's Future Launcher Preparatory Program (FLPP3) namely the study "Upper Stage Attitude Control Framework" with contract number 4000110733/14/F/JLV. The authors thank the study lead and technical officers, Adriana Sirbi and Samir Bennani, for their support and encouragement.

Appendix A. Supplementary data

Supplementary data related to this article can be found at <http://dx.doi.org/10.1016/j.actaastro.2018.06.055>.

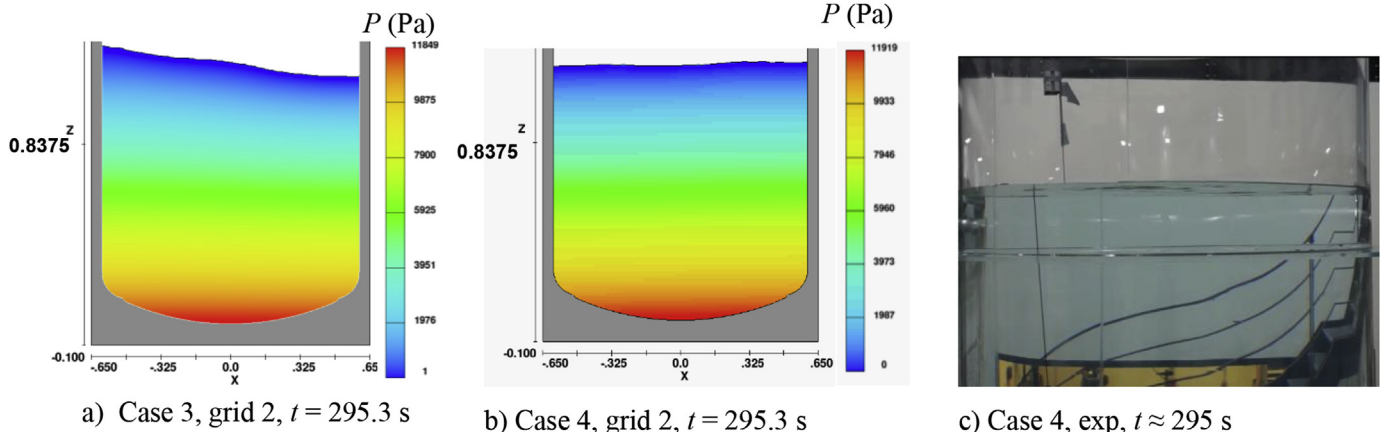


Fig. 24. Fluid pressure contours of the natural damping and active damping simulations at cases 3 and 4 and image of the surface shape of the experiment at case 4.

References

- [1] A. Frank, P. Lutz, D. Regenbrecht, The test centre Lampoldshausen and its role in Ariane 6 development and beyond, SpaceOps 2016 Conference, AIAA 2016-2503, 2016.
- [2] J.-M. Sannino, J.-F. Delange, V. De Korver, A. Lekeux, B. Vieille, VINCI propulsion system: transition from Ariane 5 ME to Ariane 6, AIAA Propulsion and Energy Forum 2016, AIAA 2016-4678, 2016.
- [3] F.T. Dodge, The New "Dynamic Behaviour of Liquids in Moving Containers, Southwest Research Institute, 2000.
- [4] H.N. Abramson, Dynamic Behaviour of Liquids in Moving Containers with Applications to Propellants in Space Vehicle Fuel Tanks, (1966) NASA-SP-106.
- [5] F. De Rose, Modeling of upper stage dynamics including fuel sloshing and utilization for future space vehicles, 6th European Conference for Aeronautics and Space Sciences (EUCASS), Paper 219, 2015.
- [6] P. Behruzi, F. de Rose, P. Netzlaf, H. Strauch, Ballistic Phase Management for Cryogenic Upper Stages, DLRK Tagungsband, Deutsche Gesellschaft f. Luft- und Raumfahrt, 978-3-932182-74-7, 2011, pp. 1343–1351.
- [7] P. Behruzi, D. Rosascio, G. Lapilli, D.R. Kirk, H.-J. Zachrau, Spheres tether slosh free flyer experiment on ISS, submitted for publication, AIAA Propulsion and Energy Forum, July 2018 AIAA-2018-4939.
- [8] J.R. Wertz, Spacecraft Attitude Determination and Control, Springer, 1978.
- [9] C.W. Hirt, J.M. Sicilian, A porosity technique for the definition of obstacles in rectangular cell meshes, Proceedings of the Forth International Conference on Ship Hydrodynamics, National Academy of Sciences, Washington DC, September 1985.
- [10] H. Strauch, K. Luig, S. Bennani, Model based design environment for launcher upper stage GNC development, Workshop on Simulation for European Space Programmes (SESP), ESA/ESTEC, Noordwijk, The Netherlands, March 2015, <http://arxiv.org/abs/1801.09950>.
- [11] C. Jetzschmann, H. Strauch, S. Bennani, Model based active slosh damping experiment, 10th International ESA Conference on Guidance, Navigation & Control Systems, ESA/ESTEC, Salzburg, Austria, June 2017, <http://arxiv.org/abs/1801/10017>.
- [12] M. Konopka, F. De Rose, T. Arndt, C. Jetzschmann, H. Strauch, N. Darkow, J. Gerstmann, Large-scale tank active sloshing damping simulation and experiment, Space Propulsion 2016 Conference, Paper SP2016-3124604, <http://elib.dlr.de/105017/>.
- [13] J. Gerstmann, M. Konopka, Cryo-laboratory for test and development of propellant management technologies, Space Propulsion 2016 Conference, Paper SP2016-3124996, <http://elib.dlr.de/105014/>.
- [14] J. Gerstmann, T. Arndt, J. Klatte, P. Behruzi, Cryo-laboratories for test and development of propellant storage and management technologies, Ground-based Space Facilities Symposium, CNES, June 2013 Paris, <http://elib.dlr.de/87258/>.
- [15] C.W. Hirt, B.D. Nichols, Volume of fluid (VOF) method for the dynamics of free boundaries, *J. Comput. Phys.* 39 (1981) 201–225.
- [16] Y. Saad, Iterative Methods for Sparse Linear Systems, PWS Publishing Company, 1996.
- [17] K. Zhou, J.C. Doyle, Essentials of Robust Control, Prentice-Hall, 1998.
- [18] Z. Zhou, H. Huang, Constraining surface model for large amplitude sloshing of the spacecraft with multiple tanks, *Acta Astronaut.* 111 (2015) 222–229.